PHYSICAL REVIEW B **69**, 165407 (2004)

Transition from localized surface plasmon resonance to extended surface plasmon-polariton as metallic nanoparticles merge to form a periodic hole array

W. A. Murray,[1] S. Astilean,[2] and W. L. Barnes[1]
[1]*School of Physics, University of Exeter, Exeter, EX4 4QL, United Kingdom*
[2]*Optics and Spectroscopy Department, Faculty of Physics, 3400 Cluj Napoca, Romania*
(Received 31 October 2003; published 19 April 2004)

We present results of experiments to determine the dispersion of the plasmon modes associated with periodic silver nanoparticle and nanohole arrays fabricated using an extension of the nanosphere lithography technique. Ordered monolayers of polystyrene nanospheres were used as a deposition mask through which silver was deposited by thermal evaporation, subsequent removal of the nanospheres thus leaving an array of metallic nanoparticles. By reactive-ion etching of the nanospheres in an oxygen plasma prior to silver deposition, arrays consisting of particles of increasing size were fabricated. The extremities of the particles eventually merge to create a continuous metallic network perforated by subwavelength holes, thus allowing a study of the particle-hole transition. Combining optical measurements of transmittance and reflectance with information gained using scanning electron microscopy, three separate regimes were observed. For low etch times the samples comprise mainly individual nanoparticles and the optical response is dominated by localized surface plasmon resonances that show no dispersion. As the etch time is increased almost all of the nanoparticles merge with adjacent particles, although many defects are present—notably where some particles fail to merge, a small gap being left between them. The presence of these defects prevents an abrupt structural transition from metallic nanoparticles to a continuous metallic film perforated by an array of nanoholes. The presence of such gaps also results in dispersion data that lack clearly defined features. A further increase in etch time leads to samples with no gaps: instead, a continuous metal film perforated by a nanohole array is produced. The optical response of these structures is dominated by extended surface plasmon-polariton modes.

DOI: 10.1103/PhysRevB.69.165407 PACS number(s): 78.67.−n, 73.20.Mf, 81.07.−b

I. INTRODUCTION

The optical properties of metal films patterned with features of submicron dimensions are dominated by the surface plasmon[1] modes these structures support.[2] In particular two very different regimes are encountered, one applying to isolated noble metal nanoparticles, the other to continuous noble metal nanostructures. Metallic nanoparticles support localized surface plasmon resonances while extended surface plasmon-polariton modes are found on continuous noble metal films. Many studies have separately explored these localized and extended regimes: here, we look at the transition from one regime to the other. Given the contrasting nature of the surface plasmon modes involved it is not *a priori* obvious what character this transition will take. We describe the fabrication of a variety of different sample structures and report results of measurements that explore independently both the structural transition from nanoparticle array to nanohole array and the evolution of the surface plasmon modes they support.

When visible light at an appropriate frequency is incident on a noble metal nanoparticle the spatially confined conduction electrons undergo a coherent oscillation known as the localized surface plasmon resonance (LSPR).[3] The spectral position and width of the LSPR is governed by the geometry of the particle, the dielectric functions of both the metal and surrounding media, interparticle interactions, and polarization of the incident light.[3,4] The LSPR leads to a substantial electromagnetic field enhancement relative to the incident field that plays an important role in surface-enhanced Raman scattering (SERS),[5–7] near-field microscopy,[8] and surface-enhanced fluorescence.[9,10] Exploring the properties and underlying physics of individual nanoparticles continues to be an area of keen activity, in part because the underlying physics has still to be fully explored and in part due to the many potential applications. The sensitivity of the LSPR to changes in particle shape and the manner in which adjacent particles interact are particularly important and have been the subject of many recent investigations,[11–14] nonetheless, it is the resonances of individual nanoparticles that usually dominate.

In contrast the electron plasma oscillation at the interface between a continuous metal film and a dielectric, known as the surface plasmon polariton (SPP), is extended in nature and, for a planar metal-dielectric interface, cannot be excited by incident light. This is because for a given frequency the momentum (wave vector) associated with a SPP mode is always greater than that of a photon.[15] The introduction of texture that is periodic on the scale of the wavelength of the incident light onto the surface enables photons to scatter, thus providing them with additional momentum that enables coupling between light and the SPP mode.

Despite a long history, the topic of surface plasmons continues to yield new insight into the interaction between nanostructured metals and light. In addition to allowing light to couple to surface plasmon modes, wavelength-scale periodic texture can also be used to construct photonic surfaces for SPPs. This has led to both the demonstration of a full photonic band gap for SPPs (Ref. 16) and a means to control their propagation.[17] SPPs are also involved in the observation of enhanced transmission through otherwise opaque me-

tallic films perforated with a periodic array of subwavelengths holes.[18,19] A key aspect of these developments is that not only does the introduction of wavelength-scale structure introduce a richness into the resulting surface plasmon modes, it also allows incident light to be coupled into and out of these modes.

Nanoparticles that form an array of fixed period will have edges that get closer together as the size of the particles increases so that one might expect the surface plasmon modes of the individual particles to interact with each other. Such an interaction might then lead to a soft transition from individual particle to continuous film behavior; as we will show below, this is not what happens. The work presented here explores the transition through an experimental examination of the dispersion of the surface plasmon modes as the nanoparticles of an array increase in size, eventually merging to form a nanohole array. Dispersion maps were obtained by measuring the optical transmittance as a function of frequency and in-plane wave vector. These data were correlated with images of the arrays obtained using scanning electron microscopy (SEM). In this way we were able to explore the transition in behavior from the nanoparticle response, dominated by LSPR modes, to the hole-array response, dominated by extended SPP modes.

II. SAMPLE FABRICATION

Samples were fabricated using the nanosphere lithography technique as developed elsewhere.[4] In the first step chemical treatment of the substrate (fused silica, 25 mm$\times$25 mm $\times$1.5 mm) was used to render its surface hydrophilic. This was achieved by soaking in a solution of sulphuric acid/hydrogen peroxide (3:1) for a minimum of 2 h. The substrates were then rinsed in ultrapure water followed by immersion and ultrasonication in a solution of ultrapure water/ammonium hydroxide/30% hydrogen peroxide (5:1:1) and sonicated for 1 h. Finally the substrates were thoroughly rinsed in ultrapure water and stored under ultrapure water until required. After removal from the water the substrates were dried in air at a temperature of 60 °C. Next, fresh ultrapure water was deposited and dispersed across the substrate, the amount of water used depending on the concentration of the colloidal solution and the nanosphere diameter to be used. A colloidal nanosphere solution (390 nm diameter, 4% solids from Duke Scientific Corps) was deposited onto the water film and dispersed by a gentle tipping and rotation of the sample until an even concentration was present across the substrate. Typical volumes used when ordering 390-nm-diam nanospheres were 100 μl of water and 8 μl of solution. Finally, the samples were dried in an oven at 60 °C for $\sim$1 h.

As the water evaporates the nanospheres self-assemble into a hexagonally close-packed monolayer array suitable for use as a lithographic mask. An example of a nanosphere array formed with 390-nm-diam spheres is shown in Fig. 1. The monolayer region (outlined) covers an area of $\sim$3 cm^2 and consists of randomly oriented monocrystalline domains, the largest single domain being $\sim$10 mm^2 in area. Surrounding the monolayer region are a variety of multilayer regions.

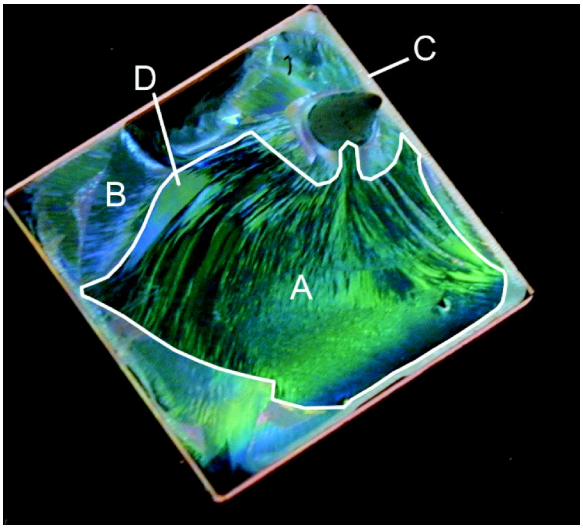

FIG. 1. Digital photo of a nanosphere array formed from 390-nm-diam polystyrene spheres with (A) monolayer region, (B) multilayer regions, (C) nanosphere wall, and (D) single-monolayer domain indicated.

At the edge of the substrate a wall of nanospheres up to 1 mm across and up to 30 nanospheres thick is formed during the initial stages of the drying procedure. The final stage of the process was to thermally evaporate silver through the nanosphere arrays. Subsequent nanosphere removal by ultra sonication in dichloromethane left an array of triangular silver nanoparticles. In all the samples discussed here 50 nm of silver was deposited.

In order to use the same basic technique to make arrays of larger nanoparticles and nanohole arrays, the nanospheres were subjected to a reactive ion etch using an oxygen plasma, prior to evaporating the silver. Haginoya *et al.* were the first to incorporate this extra step, successfully fabricating hole arrays in silicon by evaporating a Pt-Pd resist across an etched nanosphere array.[20] By incrementing the etch time in 10-s steps from 50 to 120 s, the diameter of the nanospheres is steadily reduced, resulting in samples with metallic nanoparticles of increasing size until they eventually merge to form hole arrays with a period identical to that of the particle array. The process is shown schematically in Fig. 2.

III. RESULTS AND DISCUSSION

A. SEM images

In Fig. 3 we show SEM images of (a) a nanoparticle array formed without etching the nanospheres, (b), a nanoparticle/nanohole intermediate structure, and (c) an array of 300-nm-diam holes. The diameter of the nanospheres prior to etching was 390 nm, resulting in a periodicity $\lambda_G = 338$ nm. The features caused by the presence of defects in the crystalline structure, such as vacancies, slip dislocations, and variations in nanosphere diameter, are most apparent in the nanoparticle arrays, Fig. 3(a); nanowires and ''bow-tie''-shaped particles are produced. For the nanoparticle arrays these defects seem to have little effect on the overall optical response. However,

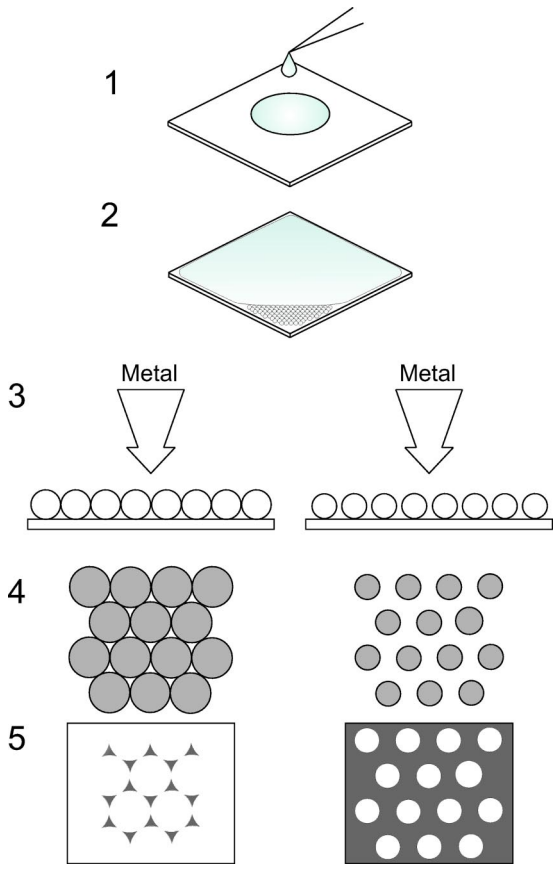

FIG. 2. Schematic of fabrication process. (1) Drop pipette colloidal solution, (2) ordering of nanospheres as fluid evaporates, (3) silver evaporation onto nonetched (left) and etched (right) nanosphere arrays, (4) plan view of arrays prior to sphere removal, and (5) particle array (left) and hole array (right) after nanosphere removal.

as the nanospheres are etched the influence of structural defects on the optical response becomes significant. Now even small variations in the nanosphere diameter will lead to a gradual rather than a sudden change as the etch time is increased; some nanoparticles will merge while others will remain isolated. This is seen in Fig. 3(b) where there are gaps and channels in the metal film surrounding what would otherwise be holes. The gaps and channels no longer appear after the samples have been etched further, as shown in Fig. 3(c). Here a continuous network of metal perforated with an array of nanoholes approximately 300 nm in diameter has been produced; there are no gaps and no isolated nanoparticles.

B. Optical characterization

To obtain optical transmittance data a collimated beam (divergence ~0.5°) from a tungsten halogen lamp was directed onto the samples. A monochromator was used to spectrally filter the incident light (spectral width ~2 nm), while a mechanical chopper modulated the intensity of the incident light so as to allow phase-sensitive detection of the zero-order transmitted and reflected beams. Further, a beam splitter redirected a small fraction of the incident beam onto a second detector to allow source fluctuations to be taken into account. Finally, a polarizer was placed in the incident beam so that the polarization state of the incident light could be controlled.

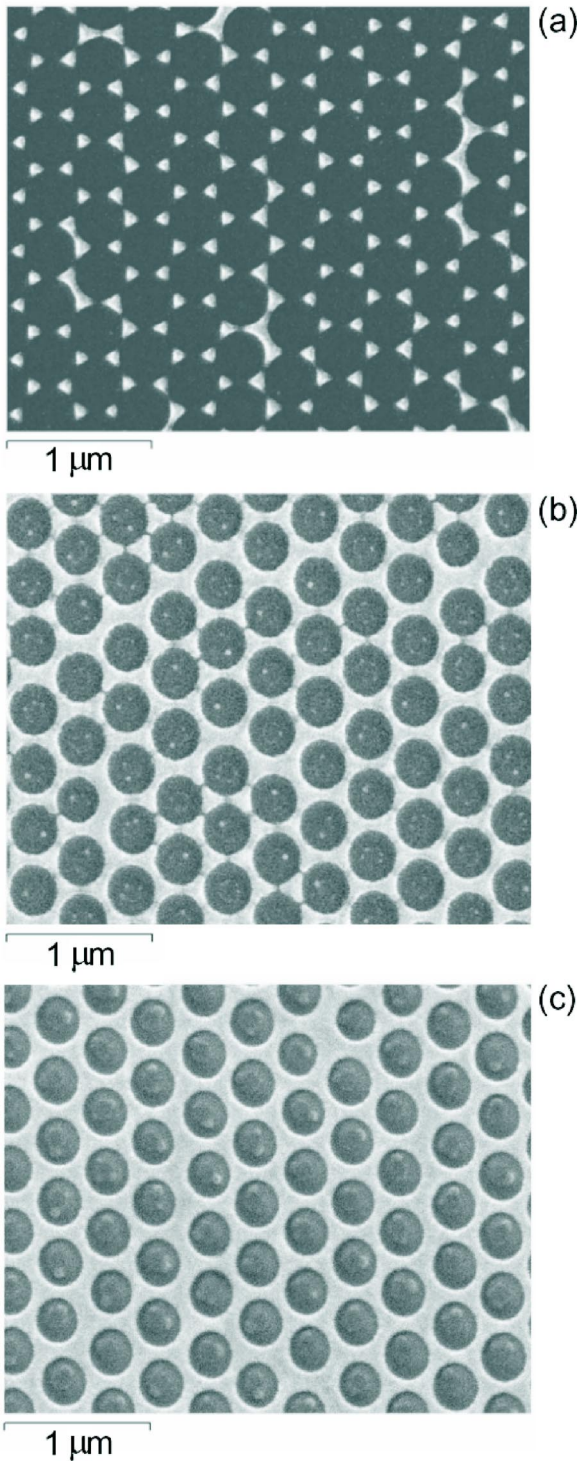

FIG. 3. SEM images of (a) nanoparticle array formed without etching the nanosphere array, (b) intermediate structure formed after etching the nanosphere array for 70 s, and (c) hole array formed after etching the nanosphere array for 120 s.

To understand the optical behavior of the periodic nanostructures we wished to build up dispersion maps from the

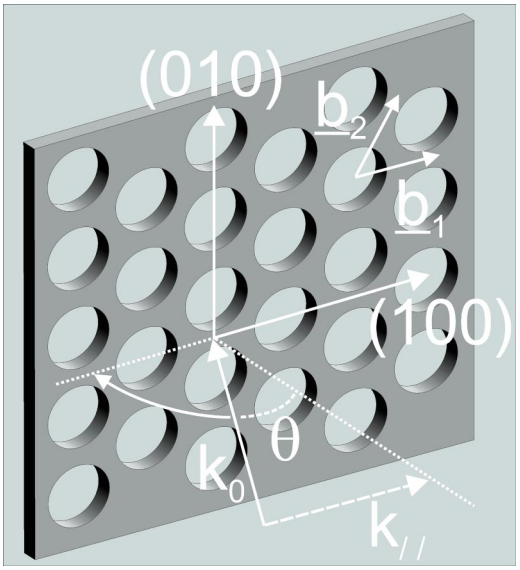

FIG. 4. Schematic illustrating the orientation of the hole array relative to coordinate axes and Bragg vectors $\mathbf{b}_1$ and $\mathbf{b}_2$ where θ is the angle of incidence, $\mathbf{k}_0$ is the incident wave vector, and $\mathbf{k}_{\|}$ is the in-plane wave vector.

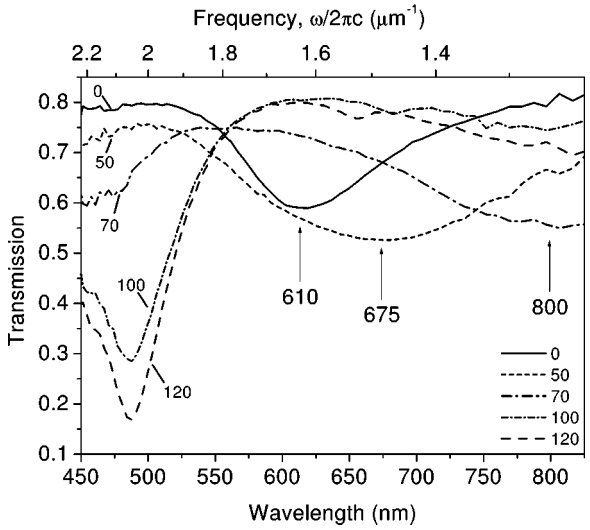

FIG. 5. Transmission spectra for *p*-polarized light with $k_{\|}/2\pi = 0$ from samples etched for 0 s, 50 s, 70 s, 100 s, and 120 s. Arrows indicate positions of the localized surface plasmon resonance.

transmittance data. To do this it is necessary to collect data not only as a function of the frequency ω, but also as a function of the in-plane wave vector $\mathbf{k}_{\|}$. The in-plane wave vector is the component of the incident wave vector $\mathbf{k}_0$ in the plane of the sample. Varying the in-plane wave vector was achieved by mounting the sample on a motor-driven rotating stage and choosing angles of incidence appropriate for each in-plane wave vector value for which data were to be recorded. Figure 4 shows the coordinate axes, together with the axis of rotation used, the (0,1,0) axis. With this choice of rotation axis the in-plane wave vector $\mathbf{k}_{\|}$ was always in the (1,0,0) direction. Measurements were made for both *p*- and *s*-polarized incident light. At normal incidence the electric field (*E* field) for *p*-polarized light is parallel to the (1,0,0) axis: for *s*-polarized light it is parallel to the (0,1,0) axis. Upon rotation of the sample about the (0,1,0) axis, *p*-polarized light has a component of the *E* field normal to the interface whereas the *E* field for *s*-polarized light remains parallel to the interface for all incident angles. The samples were initially oriented so that one of the Bragg vectors associated with the periodic structure was in the plane of incidence. This is known as the conical mount and corresponds to an azimuthal angle $\varphi = 0°$ [the azimuthal angle φ defines rotation about the (0,0,1) axis with $\varphi = 0°$ along the (1,0,0) axis].

Before looking at the acquired dispersion scans it is instructive first to look at some individual transmittance spectra. Figure 5 shows the transmittance for normally incident light for samples ranging from arrays of well-isolated nanoparticles to nanohole arrays; they were fabricated using etch times of 0 s, 50 s, 70 s, 100 s, and 120 s. As the etch time is increased the nanoparticles increase in size so that while the center-to-center particle distance remains fixed the extremities of neighboring particles become closer. For the well-isolated nanoparticle array (etch time 0 s), the transmittance shows a clear minimum at 615 nm, attributed to the ensemble-averaged LSPR. As the etch time is increased this minimum shifts to longer wavelengths, occurring at 675 nm for a 50-s etch and at ~800 nm for a 70-s etch, this behavior being consistent with data collected from many samples fabricated with a variety of etch times from 0 s to 70 s. This redshift of the LSPR for increasing particle size is well known and is due to the increasing effect of radiation damping as particle size increases.

A shift in the resonant wavelength is also expected to arise from a change in the dipolar coupling between nanoparticles as their separation decreases. For pairs of nanoparticles a redshift in the position of the LSPR is observed as particle separation decreases when the polarization of the incident light is parallel to the interparticle axis while a blueshift occurs for the orthogonal polarization.[21] However, the influence of dipolar interactions is more complex with periodic assemblies of nanoparticles. Haynes *et al.* have observed a blueshift in the LSPR position with a reduction in particle separation when the particles are contained within both square and hexagonal arrays.[22] There are thus likely to be competing processes involved in producing a shift in the position of the LSPR; in our case, the dominant effect appears to be the increase in size of the nanoparticles.

As described above, transmittance measurements obtained for a matrix of frequency and in-plane wave vector values allow a dispersion map to be produced. Figure 6 shows *p*-polarized transmission dispersion scans from the nanoparticle (a), intermediate (b), and nanohole (c) arrays described earlier. The strong, nondispersive absorption (dark) feature centered at a frequency of 1.63 μm^{-1} (615 nm) in Fig. 6(a) is characteristic of the ensemble-averaged LSPR. The dispersion scan for the intermediate structure shows ill-defined features consistent with the random nature of the defect-related discontinuities in the silver film; see Figs. 3(b) and 6(b). The dispersion data change dramatically when the etch time is

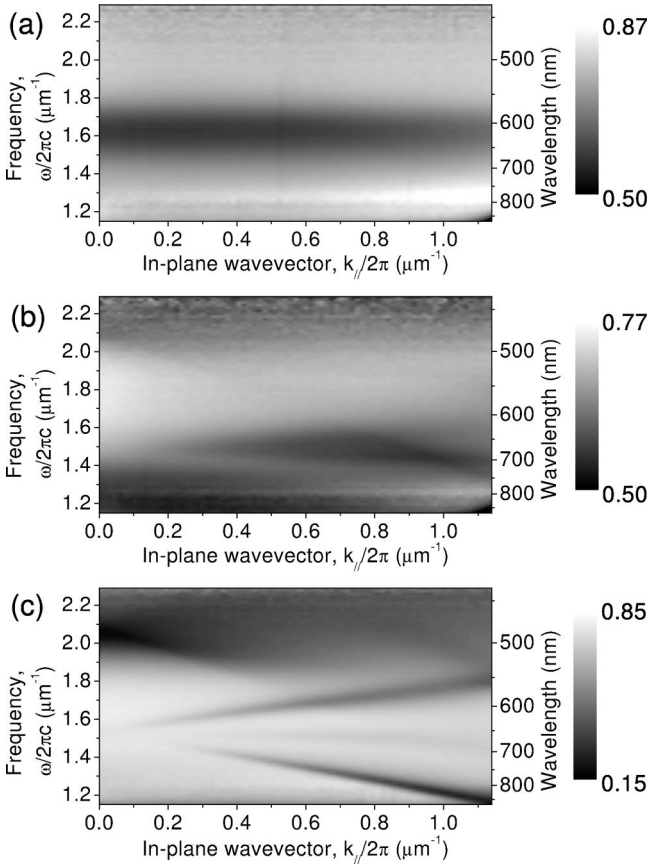

FIG. 6. Measured transmittance as a function of in-plane wave vector and frequency in the form of a greyscale diagram for *p*-polarized light incident upon the (a) nanoparticle array, (b) intermediate structure, and (c) hole array imaged in Fig. 3.

increased such that a perforated thin-film structure is produced that does not have any discontinuities. The transition is clearly illustrated in Figs. 6(c) and 5 with the appearance of a strong extinction feature centered at $\omega/2\pi c = 2.05\ \mu\mathrm{m}^{-1}$ for normal incidence ($k_{\|}/2\pi = 0\ \mu\mathrm{m}^{-1}$) and three modes intersecting at $\omega/2\pi c = 1.53\ \mu\mathrm{m}^{-1}$, also for normal incidence. The frequency at which the modes intersect at the $k_{\|}/2\pi = 0$ axis rises as the hole diameter is reduced, evident in Fig. 5 where a slight dip is observed in the transmittance from the samples etched for 100 s and 120 s at $\omega/2\pi c = 1.46\ \mu\mathrm{m}^{-1}$ and $\omega/2\pi c = 1.53\ \mu\mathrm{m}^{-1}$, respectively. Results (not shown) obtained from samples etched for as long as 180 s confirm this behavior.

C. Discussion

To help identify the physical origin of the modal features seen in Fig. 6(c) we show the same data in Fig. 7, but now superpose the dispersion of scattered surface plasmon polaritons and scattered light lines. The light line defines the maximum wave vector $k_{0\|}$ an incident photon may possess in the plane of the sample (grazing incidence) and in a dielectric medium of real permittivity ε_1 is given by

$$k_{0\|} = \frac{\omega}{c}\sqrt{\varepsilon_1}, \tag{1}$$

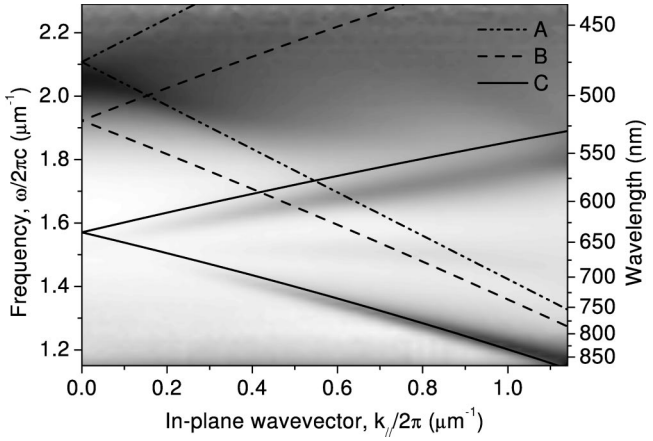

FIG. 7. Superimposed upon the data from Fig. 5(c) (A) the diffracted ($\pm 1,0$) silica light lines (dotted lines) and (B), (C) modeled dispersion of grating coupled ($\pm 1,0$) SPP modes associated with a planar silver-silica interface. The dashed lines (B) correspond to the SPP dispersion on a semi-infinite slab whereas the solid lines (C) correspond to the SPP dispersion on a 12.5-nm-thick slab with the second silver interface bounded by air.

where c is the speed of light in vacuum and ω is the angular frequency. As a first approximation the dispersion of the SPP mode is modeled using the dispersion relation for a single planar interface:[15]

$$k_{\mathrm{SPP}} = \frac{\omega}{c}\left(\frac{\varepsilon_1\varepsilon_2}{\varepsilon_1+\varepsilon_2}\right)^{1/2}, \tag{2}$$

where k_{SPP} is the magnitude of the surface plasmon-polariton wave vector and ε_2 is the frequency-dependent relative permittivity of silver. For typical values of ε_2 in the visible, $k_{\mathrm{SPP}} > k_0$ so that, as noted in the Introduction, the coupling of incident light to the SPP is not possible unless the wave vector of the incident light is enhanced, in our case by scattering off the periodic structure. The in-plane wave vector $\mathbf{k}_{\|}$ of the incident radiation is modified when compared to that of the scattered radiation by the reciprocal lattice vector $\mathbf{G}$. When the coupling condition

$$\mathbf{k}_{\mathrm{SPP}} = \mathbf{k}_{\|} + \mathbf{G} \tag{3}$$

is fulfilled the transmittance and reflectance of light by the structure will be modified, thus allowing observation of the modes of the structure. The diffracted light lines are found in a similar way, by applying the scattering equation (3) to the light line equation (1).

Assuming the nanospheres self-assemble into a perfectly ordered hexagonal arrangement, the resulting particle or hole array may be described using a two-dimensional primitive cell with lattice vectors $\mathbf{a}_1$ and $\mathbf{a}_2$ and an included angle of 120°. The corresponding primitive vectors of the reciprocal lattice, $\mathbf{b}_1$ and $\mathbf{b}_2$ (see Fig. 4) are equal in magnitude and map the scattering centers in reciprocal space according to the relation

$$\mathbf{G} = m\mathbf{b}_1 + n\mathbf{b}_2, \tag{4}$$

where m and n are integers (positive or negative) and $\mathbf{b}_1$ and $\mathbf{b}_2$ are defined by the relationship

$$\mathbf{b}_i \cdot \mathbf{a}_j = 2\pi\delta_{ij}, \tag{5}$$

for which $\delta_{ij}=1$ if $i=j$ and $\delta_{ij}=0$ if $i\neq j$. For our choices of sample orientation (Fig. 4) the reciprocal lattice vectors are set so that $\mathbf{b}_1=2\pi/\lambda_G(1,0,0)$ is in the plane of incidence and $\mathbf{b}_2=2\pi/\lambda_G(1/2,\sqrt{3}/2,0)$ is directed at an angle of 60° to $\mathbf{b}_1$. The component of the incident wave vector parallel to the interface is thus scattered by the combined integer multiples of $\mathbf{b}_1$ and $\mathbf{b}_2$.

The dispersion of the lowest-order $(m=\pm 1, n=0)$ scattered silica/silver interface SPP modes, calculated by employing a Drude model for the frequency-dependent dielectric function of the silver, is shown as the dashed lines in Fig. 7. The offset to higher frequencies of the modeled SPP mode when compared to that obtained experimentally may perhaps be explained by considering how the presence of the holes modifies the effective thickness of the silver layer. In contrast to a uniform metal film, the hole array is substantially permeated by air. The evanescently decaying electric field associated with the silica/silver interface SPP mode extends into the holes and also directly through the metal into the air bounding the opposite interface; the dispersion of the mode is thus altered. In the absence of an accurate model for the dispersion of SPP modes on perforated metal films we attempted to model this effect simply by using an effective thickness for a planar metal that was thinner than the film used. Using a metal film thickness of 12.5 nm gave the solid lines shown in Fig. 7 for the dispersion of the lowest-order scattered SPP modes associated with such a film. The positions of these calculated modes are in fair agreement with the experimentally derived SPP dispersion. The hypothesis is supported by the blueshift of the plasmon modes observed as the hole diameter is decreased, reducing the proportion of air within the layer relative to the amount of silver and therefore increasing the effective thickness.

It is also instructive to look at reflectance as well as transmittance since the combination can be used to infer absorption, provided no diffraction is possible. This is useful since when light is coupled to SPPs the enhanced fields associated with such modes lead to an increase in the absorption—absorption is thus another indicator of the presence of SPP modes.[19,23–25] The first-order scattered silica light lines are plotted as dotted lines in Fig. 7.[26] At frequencies below these lines, the zero-order regime, no diffraction into the far field is possible. Therefore, to account for a reduction in transmission one need only consider light that is specularly reflected and light that is absorbed by the structure. The absorbance A in this zero-order regime is inferred by simply combining the reflectance R and transmittance T via the relation $A=1-R-T$. Shown in Fig. 8 are reflectance, transmittance, and absorbance spectra at an in-plane wave vector of $k_\parallel/2\pi=0.5\ \mu\mathrm{m}^{-1}$, taken with light incident on the air/silver interface of the hole array. From the data we see that reflectance maxima (e.g., at 610 nm) are associated with the transmission minima and, by inference, absorbance maxima.

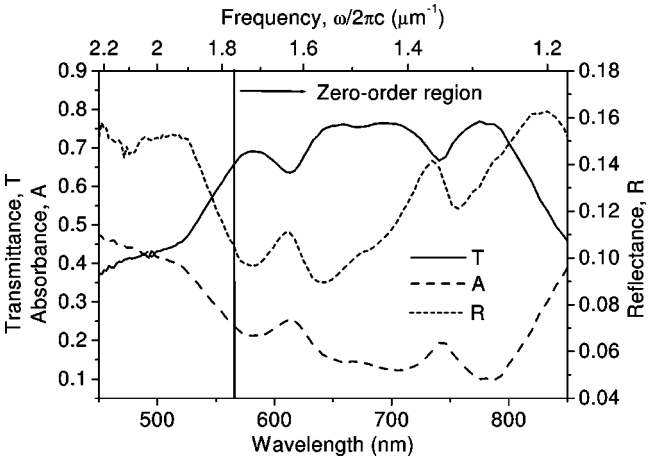

FIG. 8. Transmittance, reflectance, and inferred absorbance spectra at $k_\parallel/2\pi=0.5\ \mu\mathrm{m}^{-1}$ for p-polarized light incident upon a hole array formed with a 120-s etch.

The observation of transmission minima being associated with reflectance maxima is in marked contrast to the enhanced transmission and associated reduced reflectance seen in hole arrays in much thicker silver films.[19] The hole arrays studied previously have usually been fabricated in optically thick metal films, typically with a lattice constant somewhat higher than the diameter of the holes. In the present work, however, the metallic arrays are optically thin: this together with a low surface coverage of silver results in a far higher probability of direct transmission. This in turn leads to the possibility of interference between light that is directly transmitted and light that is first coupled into an SPP mode by scattering and then coupled back out to light, again by scattering. If this SPP-mediated light is out of phase with the directly transmitted light, then transmittance minima rather than maxima will be observed. One may expect that as the hole diameter is decreased, simply by etching the nanospheres for a time longer than 120 s, then transmittance maxima may be observed as the intensity of the directly transmitted light is reduced. From preliminary results this appears to be the case, though further investigation is needed. Similarly, the increase in the zero-order reflectance that we observe might be attributed to interference between light that is specularly reflected and that which is first coupled into the SPP and then coupled back out.

There are three further observations to make concerning the dispersion data, Fig. 6, that we cannot fully explain at this stage. First, we note that the SPP modes are only weakly coupled at normal incidence $(k_\parallel/2\pi=0)$. For incident light to generate the surface charge density associated with the SPP the mode there needs to be a component of the incident electric field perpendicular to the interface. Not being able to fulfill this condition for light normally incident on a sinusoidally modulated metal film is responsible for the lack of coupling to one of the band edges associated with an SPP band gap on such surfaces.[27] A similar reason may be behind the lack of coupling we see here for our modes at normal incidence. Second, there is a strong dip in the transmission centered at a frequency of $\omega/2\pi c=2.05\ \mu\mathrm{m}^{-1}$ at normal incidence for the hole arrays, Figs. 5 and 6(c). It is located

slightly below the frequency at which the diffracted light lines intersect, $\omega/2\pi c = 2.10\ \mu\mathrm{m}^{-1}$, and is found to be invariant in position as the hole diameter is changed. The origin of this feature is not yet clear but is associated with a reflectivity maximum and strong absorption (data not shown). Last, we note from the dispersion data the presence of a third bandlike feature centered at $\omega/2\pi c \sim 1.5\ \mu\mathrm{m}^{-1}$ that shows only weak dispersion. The origin of this feature is not clear but is perhaps due to SPP modes scattered by the second reciprocal lattice vector $\mathbf{b}_2$, the one that is not in the plane of incidence. Modeling the optical response of our structures may help elucidate these three aspects that thus far remain unclear; this is the subject of ongoing research.

IV. CONCLUSION

Using an extension of the nanosphere lithography technique in which a two-dimensional array of nanospheres is etched prior to vacuum deposition of a suitable metal, we have been able to fabricate metallic nanoparticle and nanohole arrays that exhibit very different optical responses due to the different types of plasmon modes they support. We have shown that there is an abrupt transition in the optical response of these structures from localized surface plasmon resonances to delocalized surface plasmon-polariton modes, as nanoparticles increase in size and merge to form a continuous perforated film. In contrast the SEM images show a soft transition from nanoparticles to nanohole arrays as the etch time is increased arising from the presence of a significant number of defects in the fabricated structures. This contrast between a soft transition in the SEM images and an abrupt transition in the optical response is attributed to the need for connectivity of the metal mesh before extended SPP behavior can be exhibited. Some features remain to be explained. Further investigation should not only improve our knowledge about these aspects: it may also help us to exploit these fascinating structures in a variety of applications.

ACKNOWLEDGMENT

The authors gratefully acknowledge the support of the Engineering and Physical Sciences Research Council (EPSRC).

[1] We note that for convenience we are using the term surface plasmon rather loosely—for a discussion of this point, see E. Burstein, in *Polaritons*, edited by E. Burstein and F. De Martini (Pergamon, New York, 1974), p. 1.

[2] Special issue, Appl. Phys. B: Lasers Opt. **73** (2001), all articles contained within.

[3] U. Kreibig and M. Vollmer, *Optical Properties of Metal Clusters* (Springer, Berlin, 1995).

[4] C. L. Haynes and R. P. Van Duyne, J. Phys. Chem. B **105**, 5599 (2001).

[5] G. C. Schatz and R. P. Van Duyne, in *Handbook of Vibrational Spectroscopy*, edited by J. M. Chalmers and P. R. Griffiths (Wiley, Cnichester, 2002), p. 1.

[6] S. M. Nie and S. R. Emery, Science **275**, 1102 (1997).

[7] A. Wokaun, J. P. Gordon, and P. F. Liao, Phys. Rev. Lett. **48**, 957 (1982).

[8] D. W. Pohl, in *Near-Field Optics and Surface Plasmon Polaritons*, edited by S. Kawata (Springer-Verlag, Heidelberg, 2001), Vol. 81, p. 1.

[9] H. Ditlbacher, N. Felidj, J. R. Krenn, B. Lamprecht, A. Leitner, and F. R. Aussenegg, Appl. Phys. B: Lasers Opt. **73**, 373 (2001).

[10] O. Kulakovich, N. Strekal, A. Yaroshevich, S. Maskevich, S. Gaponenko, I. Nabiev, U. Woggon, and M. Artemyev, Nano Lett. **2**, 1449 (2002).

[11] J. J. Mock, M. Barbic, D. R. Smith, D. A. Schultz, and S. Schultz, J. Chem. Phys. **116**, 6755 (2002).

[12] C. L. Haynes, A. D. McFarland, M. T. Smith, M. T. Smith, J. C. Hulteen, and R. P. Van Duyne, J. Phys. Chem. B **106**, 1898 (2002).

[13] M. Salerno, N. Felidj, J. R. Krenn, A. Leitner, F. R. Aussenegg, and J. C. Weeber, Phys. Rev. B **63**, 165422 (2001).

[14] J. P. Kottmann and O. J. F. Martin, Opt. Lett. **26**, 1096 (2001).

[15] J. R. Sambles, G. W. Bradbery, and F. Z. Yang, Contemp. Phys. **32**, 173 (1991).

[16] S. C. Kitson, W. L. Barnes, and J. R. Sambles, Phys. Rev. Lett. **77**, 2670 (1996).

[17] S. I. Bozhevolnyi, J. Erland, K. Leosson, P. M. W. Skovgaard, and J. M. Hvam, Phys. Rev. Lett. **86**, 3008 (2001).

[18] T. W. Ebbesen, H. J. Lezec, H. F. Ghaemi, T. Thio, and P. A. Wolff, Nature (London) **391**, 667 (1998).

[19] W. L. Barnes, E. Devaux, H. J. Lezec, and T. W. Ebbesen, CLEO Europe, CM-10179, Munich (2003).

[20] C. Haginoya, M. Ishibashi, and K. Koike, Appl. Phys. Lett. **71**, 2934 (1997).

[21] W. Rechberger, A. Hohenau, A. Leitner, J. R. Krenn, B. Lamprecht, and F. R. Aussenegg, Opt. Commun. **220**, 137 (2003).

[22] C. L. Haynes, A. D. McFarland, L. L. Zhao, R. P. Van Duyne, G. C. Schatz, L. Gunnarsson, J. Prikulis, B. Kasemo, and M. Kall, J. Phys. Chem. B **107**, 7337 (2003).

[23] M. Sarrazin, J. P. Vigneron, and J. M. Vigoureux, Phys. Rev. B **67**, 085415 (2003).

[24] N. Bonod, S. Enoch, L. Li, E. Popov, and M. Neviere, Opt. Express **11**, 482 (2003).

[25] I. R. Hooper and J. R. Sambles, Phys. Rev. B **67**, 235404 (2003).

[26] Note that the periodicity used to calculate the position of these lines was 325 nm and not the 338 nm expected from the sphere size. The value used was obtained from diffraction measurements on our samples. The difference is probably due to a slight distortion in our structures and possibly the packing was not fully close.

[27] W. L. Barnes, T. W. Preist, S. C. Kitson, and J. R. Sambles, Phys. Rev. B **54**, 6227 (1996).